Electronic Supplementary Information (ESI)

Passing it up the ranks: Hierarchical ion-size dependent supramolecular response in 1D coordination polymers

Debobroto Sensharma,[a] Paul Wix,[a] Amal Cherian Kathalikkattil[a] and Wolfgang Schmitt[a,*]

School of Chemistry & CRANN Institute, University of Dublin, Trinity College, Dublin 2, Ireland. E-mail: schmittw@tcd.ie; Fax: +353-1-6712826; Tel: +353-1-8963495

S1. Syntheses

S2. Powder X-ray Diffraction

S3. Thermogravimetric Analysis

S4. FTIR Spectroscopy

S5. SHAPE Analysis

S6. Single Crystal X-ray Diffraction and Structural Analysis

S7. Analysis of Non-bonding Interactions using Hirshfeld Surface Plots

S8. References

S1. Syntheses

All chemicals mentioned were used as obtained from standard commercial sources.

Synthesis of **1,** [Zn(2-tpt)(Hbtb)]·DMF: 10 mg (0.034 mmol) of $Zn(NO_3)_2·6H_2O$ was added to a slurry of 11 mg (0.035 mmol) of 2,4,6-tris(2-pyridyl)-*s*-triazine (2-tpt) and 15 mg (0.034 mmol) of 4,4',4''-benzene-1,3,5-triyl-tris(benzoic acid) (H_3btb) in 1 mL of *N,N*-dimethylformamide in a screw-top vial. The vial was agitated for a few minutes until the slurry was clarified, then heated at 100°C for four days. The product was obtained as a pale yellow crystalline solid and dried in air. Yield: 9.4 mg, 28%. CHN Analysis calculated for $C_{51}H_{42}N_8O_8Zn$ (with two constitutional DMF molecules per formula unit): C 63.79%, H 4.41%, N 11.67%; experimental: C 63.10%, H 3.76%, N 11.03%.

Synthesis of **2,** [Ni(2-tpt)(Hbtb)]·0.7DMF: 10 mg (0.034 mmol) of $Ni(NO_3)_2·6H_2O$ was added to a slurry of 11 mg (0.035 mmol) of 2,4,6-tris(2-pyridyl)-*s*-triazine (2-tpt) and 15 mg (0.034 mmol) of 4,4',4''-benzene-1,3,5-triyl-tris(benzoic acid) (H_3btb) in 1 mL of *N,N*-dimethylformamide in a screw-top vial. The vial was agitated for a few minutes until the slurry was clarified, then heated at 100°C for four days. The product was obtained as individual green single crystals, separated by hand, and dried in air. Yield: <5%.

Synthesis of **3,** [Mn(2-tpt)(Hbtb)]·1.25DMF: 7 mg (0.035 mmol) of $MnCl_2·4H_2O$ was added to a slurry of 11 mg (0.035 mmol) of 2,4,6-tris(2-pyridyl)-*s*-triazine (2-tpt) and 15 mg (0.034 mmol) of 4,4',4''-benzene-1,3,5-triyl-tris(benzoic acid) (H_3btb) in 1 mL of *N,N*-dimethylformamide in a screw-top vial. The vial was agitated for a few minutes until the slurry was clarified, then heated at 100°C for four days. The product was obtained as a pale orange crystalline solid and dried in air. Yield: 5.6 mg, 17%. CHN Analysis calculated for $C_{51}H_{46}N_8O_{10}Mn$ (with two constitutional DMF molecules and two constitutional water molecules per formula unit): C 62.13%, H 4.70%, N 11.37%; experimental: C 61.98%, H 3.75%, N 12.75%.

Synthesis of **4,** [Cd(2-tpt)(Hbtb)]·DMF: 10 mg (0.032 mmol) of $Cd(NO_3)_2·4H_2O$ was added to a slurry of 11 mg (0.035 mmol) of 2,4,6-tris(2-pyridyl)-*s*-triazine (2-tpt) and 15 mg (0.034 mmol) of 4,4',4''-benzene-1,3,5-triyl-tris(benzoic acid) (H_3btb) in 1 mL of *N,N*-dimethylformamide in a screw-top vial. The vial was agitated for a few minutes until the slurry was clarified, then heated at 100°C for four days. The product was obtained as a clear crystalline solid and dried in air. Yield: 10.0 mg, 29%. CHN Analysis calculated for $C_{51}H_{42}N_8O_8Cd$ (with two constitutional DMF molecules per formula unit): C 60.81%, H 4.20%, N 11.12%; experimental: C 60.73%, H 3.74%, N 10.66%.

S2. Powder X-Ray Diffraction

Powder XRD patterns were measured by sealing ground samples under DMF in a 0.5 mm diameter glass capillary. The capillaries were mounted and centered on a goniometer head on a Bruker APEX II diffractometer for data collection. The data were collected at 293 K using CuKα microfocus source (wavelength of 1.54184 Å) upon 360° ϕ rotational frames at 2θ values of 10° and 20°, with exposure times of 5 minutes per frame at a detector distance of 120 mm. Overlapping sections of data were combined and the data was processed using the Bruker APEX II routine XRD2 -Eval subprogram. The PXRD pattern of the bulk sample and its pattern that was calculated based on the single-crystal X-ray diffraction data (using CCDC-Mercury software package) are present overlaid. The fit between experimental and calculated patterns confirms the phase-purity of the sample and validates the provided structural model.

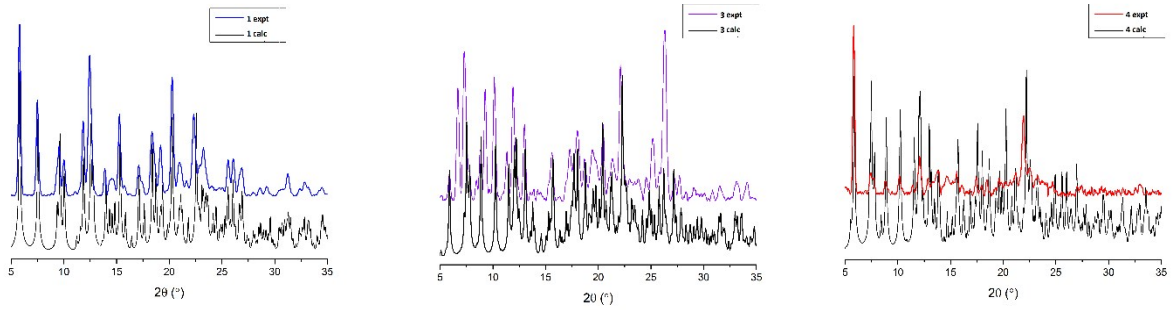

(a) **(b)** **(c)**

Figure S1: (a – c) Experimental and simulated PXRD patterns for **1**, **3,** and **4**, respectively.

S3. Thermogravimetric Analysis

Thermogravimetric analysis (TGA) was carried out using a Perkin Elmer Pyris-1 thermogravimetric analyser under a continuous flow of nitrogen. Measurements were carried out between 20°C and 600°C at a heating rate of 5°C per minute.

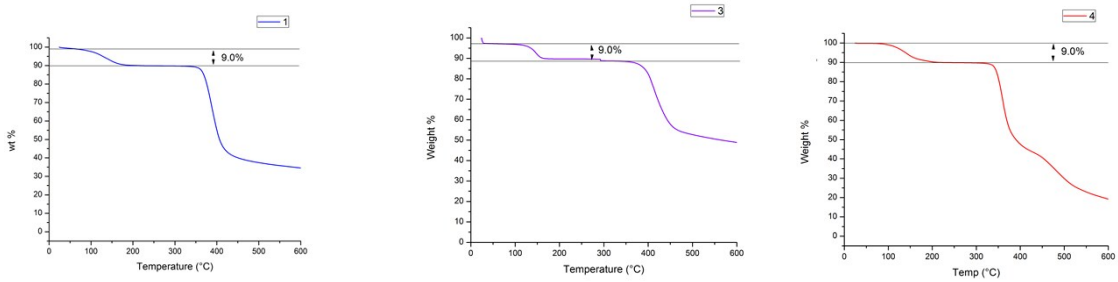

(a) **(b)** **(c)**

Figure S2: (a – c) Thermogravimetric analysis for **1**, **3**, and **4**, respectively.

S4. FTIR Spectroscopy

Infrared spectroscopy was recorded on a PerkinElmer Spectrum One FT-IR spectrometer using a universal ATR sampling accessory. Data was collected and processed using Spectrum v5.0.1 (2002 PerkinElmer Instrument LLC) software. 16 scans were collected in the range 4000-650 cm^{-1}. The range 2000-650 cm^{-1} is presented here.

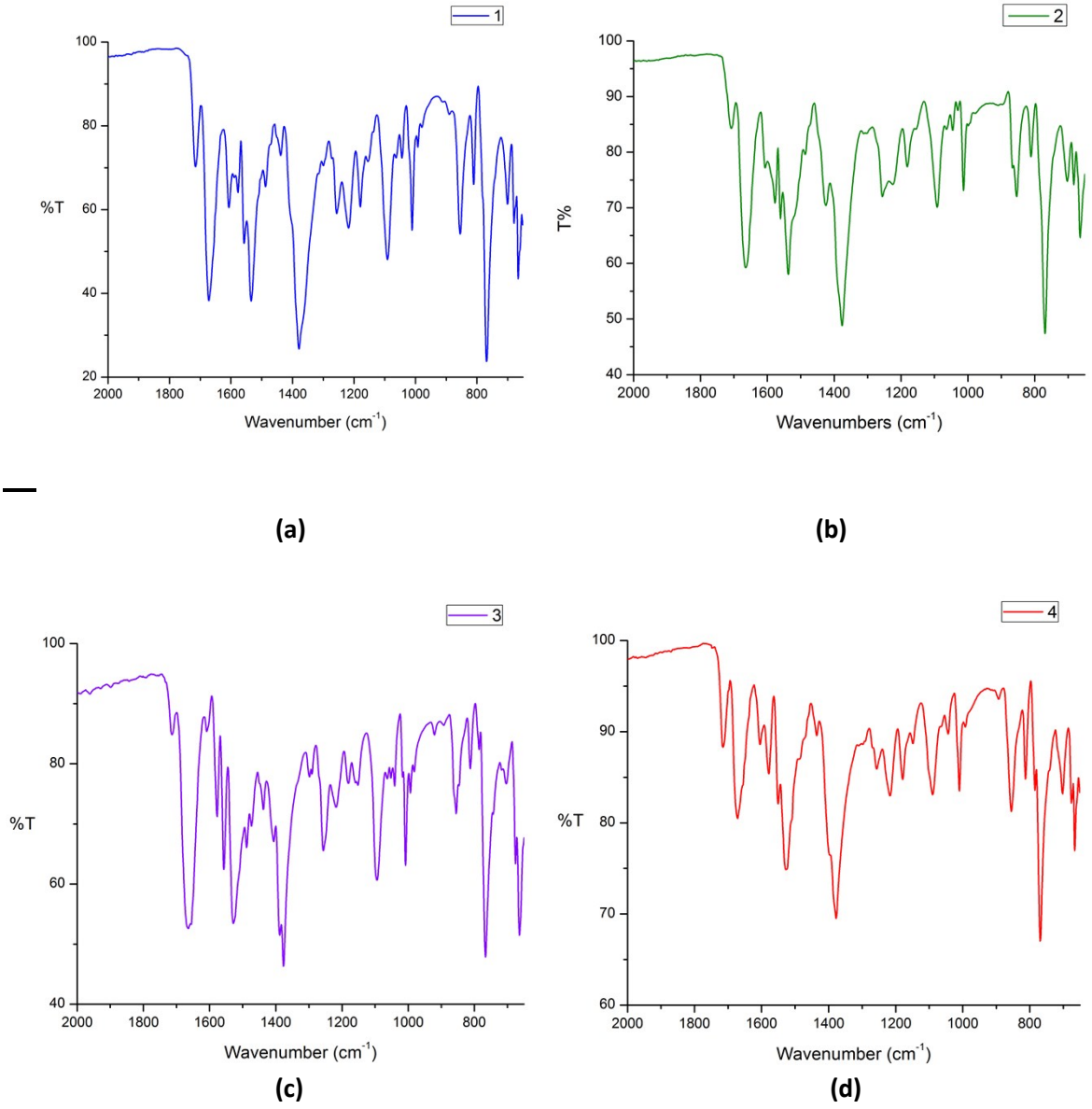

Figure S3: (a – d) FTIR spectra of compounds **1**, **2**, **3**, and **4**, respectively.

S5. SHAPE Analysis

Geometrical analysis of the coordination environment of the metal centres was performed with the program SHAPE V2.1. Calculations for selected geometries found below.

Table S1: Results of the geometrical analysis of the coordination environment with SHAPE V2.1.

1	Spherical square pyramid	Trigonal bipyramid	Vacant octahedron
	3.418	4.893	5.009
2	Octahedron	Trigonal Prism	
	4.873	8.861	
3	Capped octahedron	Capped trigonal prism	
	2.933	3.258	
4	Capped trigonal prism	Capped octahedron	
	3.312	4.566	

S6. Single Crystal X-ray Diffraction and Structural Analysis

Single crystal X-ray analysis and refinement were performed using a Bruker APEX2 Duo diffractometer. X-Ray intensity data were measured at 100K using an Oxford Cryosystem Cobra low temperature device using a MiTeGen micromount. Frames were integrated with the Bruker SAINT software package[S1] and the data corrected for absorption effects using the multi-scan method (SADABS). Structures were solved by intrinsic phasing using XT[S2] and refined with the programs Olex2[S3] and XL[S4] least squares refinement. All non-hydrogen atoms were refined anisotropically. In the case of **2** the contribution from highly disordered solvent molecules were removed using the squeeze routine (PLATON)[S5]. Electron density 'squeezed' from the structural models of compound **2** amounts to 236 per unit cell, or 29.5 per asymmetric unit. This corresponds to 0.7 constitutional DMF molecules per formula unit, and the overall formula of **2** is assigned on this basis.

Table S2: Crystallographic details.

Identification code	**1**	**2**	**3**	**4**
Empirical formula	$C_{48}H_{35}N_7O_7Zn$	$C_{47.1}H_{32.9}N_{6.7}NiO_{6.7}$	$C_{48.75}H_{36.75}MnN_{7.25}O_{7.25}$	$C_{48}H_{35}CdN_7O_7$
Formula weight	887.20	858.61	895.04	934.23
Temperature/K	100.0	100(2)	99.99	100(2)
Crystal system	monoclinic	monoclinic	monoclinic	monoclinic
Space group	C2/c	C2/c	P2/c	P2/c
a/Å	33.908(2)	34.7205(18)	16.2604(6)	16.281(3)
b/Å	17.5051(13)	17.3089(6)	17.3810(6)	17.516(3)
c/Å	15.7559(13)	15.8202(7)	30.3417(10)	30.291(4)
α/°	90	90	90	90
β/°	115.591(5)	115.923(2)	101.280(2)	100.546(3)
γ/°	90	90	90	90
Volume/Å³	8434.6(12)	8550.9(7)	8409.6(5)	8492(2)
Z	8	8	8	8
ρ_{calc}g/cm³	1.397	1.333	1.414	1.461
μ/mm⁻¹	1.325	1.093	3.088	0.576
F(000)	3664.0	3316.0	3704.0	3808.0
Crystal size/mm³	0.14 × 0.06 × 0.02	0.16 × 0.06 × 0.05	0.16 × 0.09 × 0.08	0.3 × 0.25 × 0.15
Radiation	CuKα (λ = 1.54178)	CuKα (λ = 1.54178)	CuKα (λ = 1.54178)	MoKα (λ = 0.71073)
2θ range for data collection/°	5.78 to 116.178	5.66 to 137.15	5.084 to 136.946	2.326 to 50.852
Index ranges	-37 ≤ h ≤ 37, -17 ≤ k ≤ 19, -17 ≤ l ≤ 13	-36 ≤ h ≤ 41, -20 ≤ k ≤ 20, -19 ≤ l ≤ 18	-17 ≤ h ≤ 19, -20 ≤ k ≤ 20, -36 ≤ l ≤ 35	-19 ≤ h ≤ 14, -21 ≤ k ≤ 19, -33 ≤ l ≤ 36
Reflections collected	20659	53655	58048	73384
Independent reflections	5802 [R_{int} = 0.0549, R_{sigma} = 0.0541]	7864 [R_{int} = 0.0912, R_{sigma} = 0.0508]	15442 [R_{int} = 0.0460, R_{sigma} = 0.0370]	15578 [R_{int} = 0.0714, R_{sigma} = 0.0747]
Data/restraints/parameters	5802/57/583	7864/2095/999	15442/422/1334	15578/492/1300

Goodness-of-fit on F^2	1.029	1.045	1.029	1.186
Final R indexes [I>=2σ (I)]	R_1 = 0.0623, wR_2 = 0.1664	R_1 = 0.0996, wR_2 = 0.2742	R_1 = 0.0636, wR_2 = 0.1723	R_1 = 0.1267, wR_2 = 0.2510
Final R indexes [all data]	R_1 = 0.0829, wR_2 = 0.1826	R_1 = 0.1612, wR_2 = 0.3409	R_1 = 0.0781, wR_2 = 0.1847	R_1 = 0.1881, wR_2 = 0.2798
Largest diff. peak/hole / e $Å^{-3}$	1.19/-0.67	0.48/-0.33	0.85/-0.72	2.87/-2.42
CCDC Deposition number	1852299	1852474	1852300	1852472

Table S3: Comparison of different structural features in **1-4**.

	1 – Zn	**2 – Ni**	**3 – Mn**	**4 - Cd**
Coordination	5-c	5/6-c	6/7-c	6/7-c
Denticity	Mono/mono	Mono/bi	Mono/bi	Mono/bi
Ionic Radii[S6]	0.68	0.69	0.9	1.03
Crystal Radii[S6]	0.82	0.83	1.04	1.17
Stacking modes	A,B	A,B	A,B,C	A,B,C
Stacking sequence	ABAB	ABAB	ABAC	ABAC
M-O distances	1.94	1.95	2.17 – 2.41	2.14 – 2.56
M-N distances	2.06 – 2.27	1.89 – 2.10	2.22 – 2.35	2.29 – 2.40
Shape Analysis	Square pyramidal	Octahedral	Capped Octahedral	Capped trigonal prismatic
Plane angle	41.164	14.097/48.081	45.019(47.624)/ 69.299	45.594/69.412
Hirshfeld C-C	6.8 %	5 %	5.3 %	5.3 %
Hirshfeld C-H	26.7 %	22.8 %	28.1 %	32.2 %
C-C/C-H ratio	3.9	4.6	5.3	6.1

S7. Analysis of Non-bonding Interactions using Hirshfeld Surface Plots

High-resolution Hirshfeld surfaces were generated using CRYSTAL EXPLORER[S7] for the individual repeating units of [M(Hbtb)(2-tpt)] in order to illustrate the nature of the non-covalent interactions involved in the three dimensional packing of the 1D polymer chains.

D_{norm} Plots

D_{norm} plots for 1-4 are presented here. These plots consist of a normalised contact distance between atoms interior and exterior to the Hirshfeld surface mapped on to the surface, in which blue regions correspond to contacts longer than the sum of the van der Waals' radii and red regions correspond to contacts shorter than it for the atoms involved.

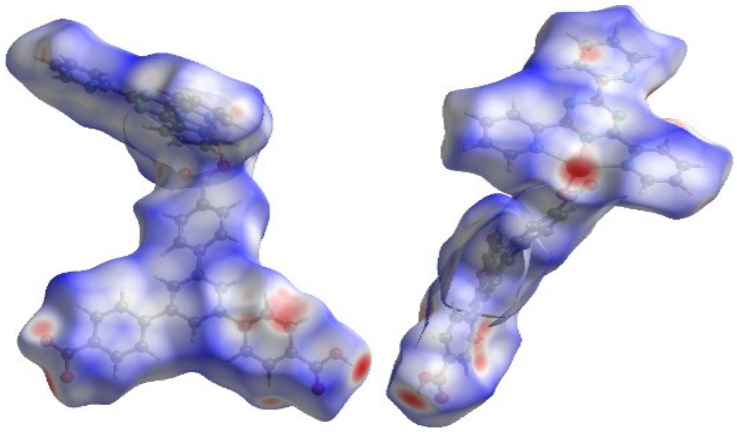

Figure S4: D_{norm} plots of **1**.

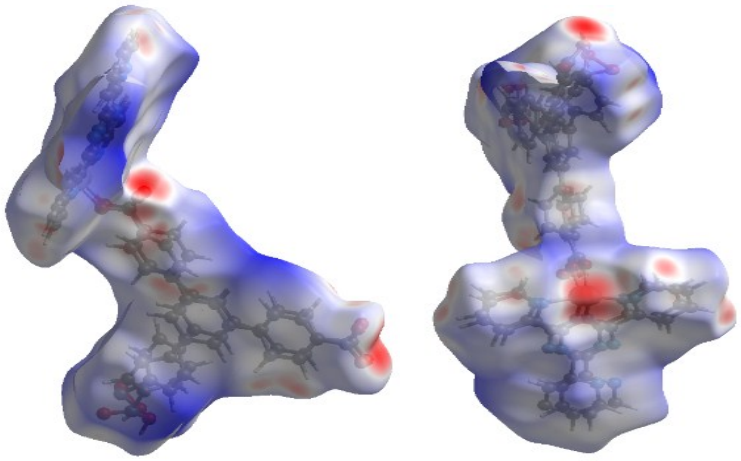

Figure S5: D_{norm} plots of **2**.

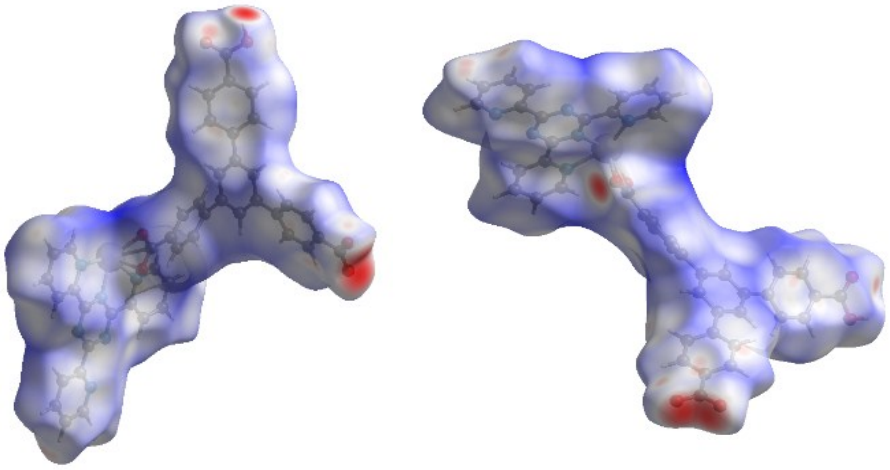

Figure S6: D_{norm} plots of **3**.

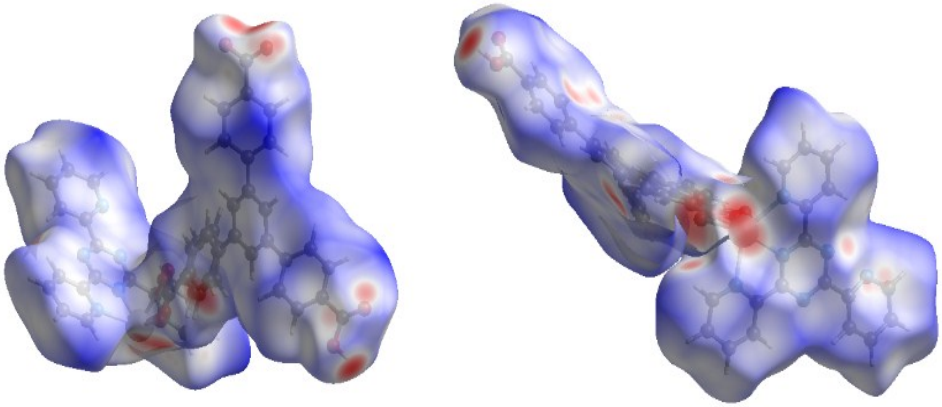

Figure S7: D_{norm} plots of **4**.

In Figs. S4-S7 the red areas of the D_{norm} plot correspond to areas that have shortened contacts due to hydrogen bonding and π-π interaction. These can be distinctly identified in the following parts of the unit – the pendant carboxyl proton, which is strongly involved in H-bonding interactions in each case, oxygen atoms on the coordinating carboxylate groups which interact with the aforementioned protons in H-bonds, parts of the aromatic rings involved in π-π stacking, and diffuse short contacts around the metal centre and aryl protons which interact weakly with disordered solvent molecules.

Fingerprint Plots

The fingerprint plot of a Hirshfeld surface consists of the external contact distance (Å) plotted against internal contact distance for every point on the surface.[S8] Interactions between similar species (e.g. C-C (π-π) interactions) appear along the diagonal since the Hirshfeld surfaces of two identical interacting species must coincide exactly halfway in between them. The asymmetry in the overall fingerprint plots of **1-4** is due to the presence of contacts to solvents, all of which have been considered external to the Hirshfeld surfaces in this work.

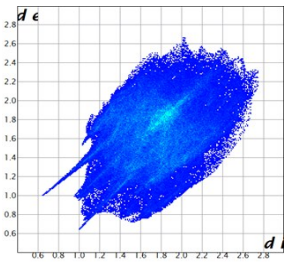

(a)

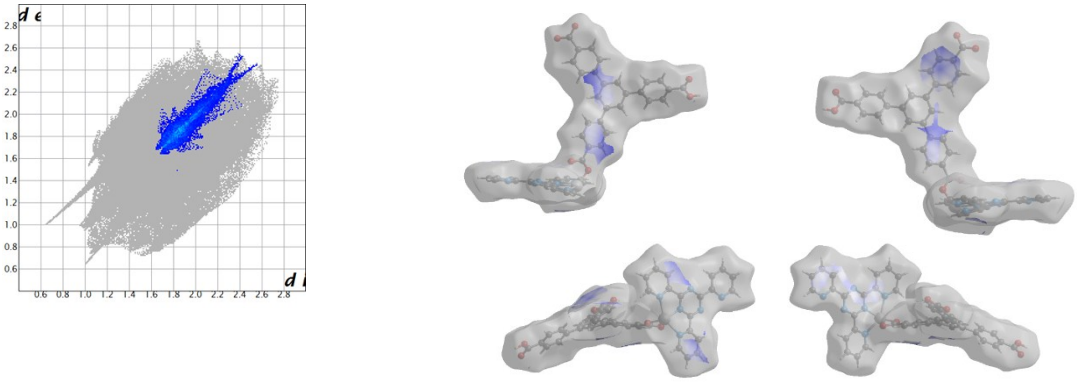

(b)

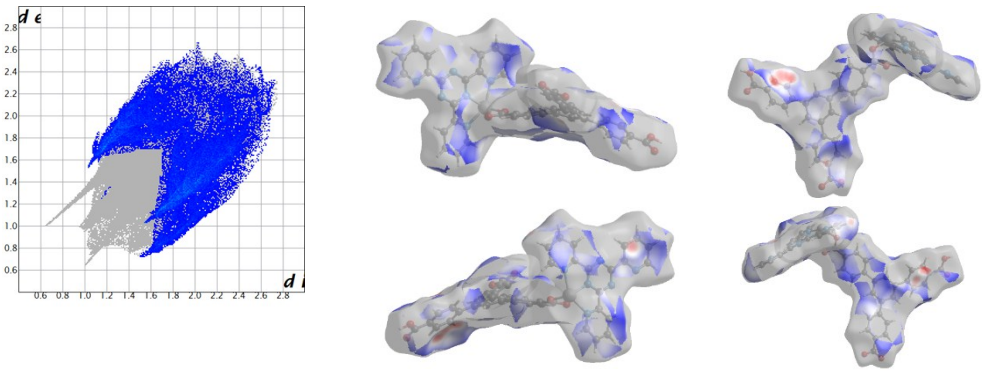

(c)

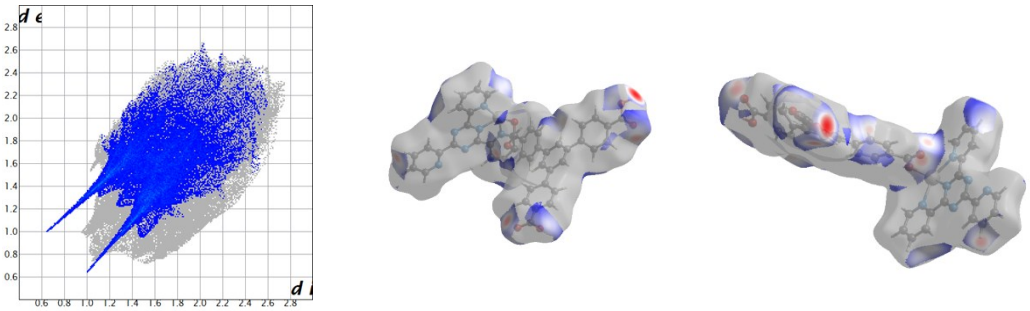

(d)

Figure S8: Fingerprint plots and corresponding regions plotted on the Hirshfeld surface for **1**: (a) Overall fingerprint plot, (b) C-C decomposed fingerprint and Dnorm plots, (c) C-H decomposed fingerprint and Dnorm plots (reciprocal contacts included), (d) O-H decomposed fingerprint and Dnorm plots (reciprocal contacts included).

In Fig. S8, decomposed fingerprint plots show that π-π, C-H···π, and H-bonding interactions all play a major role in the supramolecular ordering of 1D chains relative to each other. The decomposed C-C plot corresponds to π-π interactions, which cover 6.8% of the total Hirshfeld surface. The plot locates these at d(ext)=d(int)≅1.8 Å, which agrees well with face-on π-π stacking. The coloured region of the decomposed Dnorm surface correspond with A and B type stacking as detailed in the main manuscript. The decomposed fingerprint for C-H and H-C short contacts is shown in Fig. S14(c), and the contacts are located on the peripheries of the stacking phenyl rings (C-H···π interactions), accounting for 26.7% of the overall Hirshfeld surface. Hydrogen bonds are evaluated using the decomposed O-H and H-O fingerprint plot, which shows distinct 'wings' at ca. d(ext)=0.7 Å, d(int)=1.1 Å and d(int)=0.7 Å, d(ext)=1.1 Å, and are localised on the surface at distinct short contact regions around the pendant protonated carboxylate group and the oxygen atoms of the bound carboxylate. These cover 19.8% of the Hirshfeld surface.

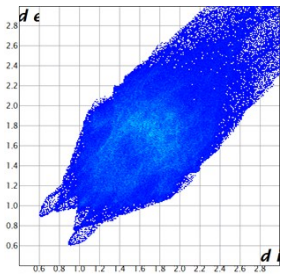

(a)

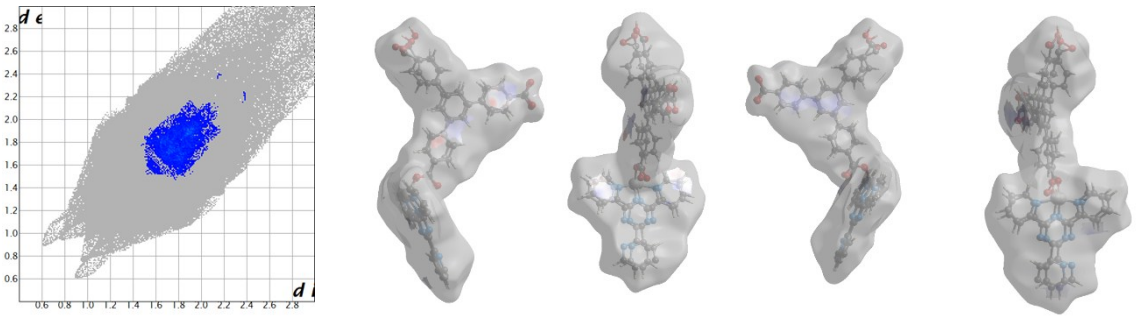

(b)

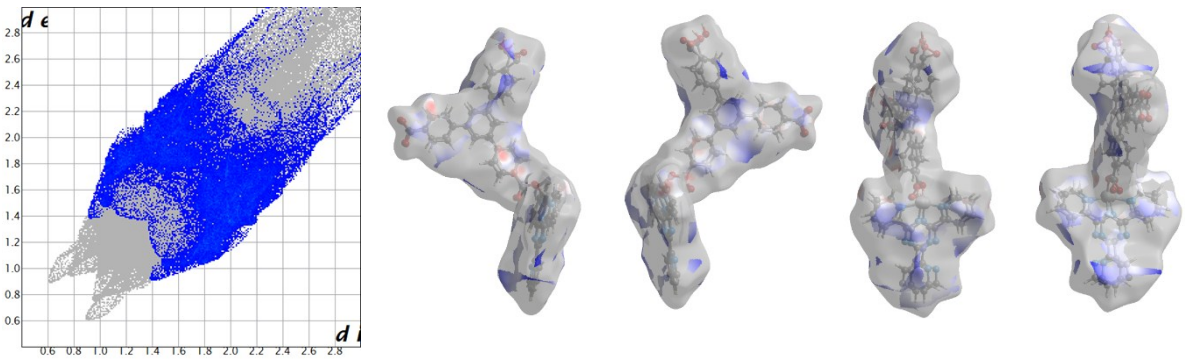

(c)

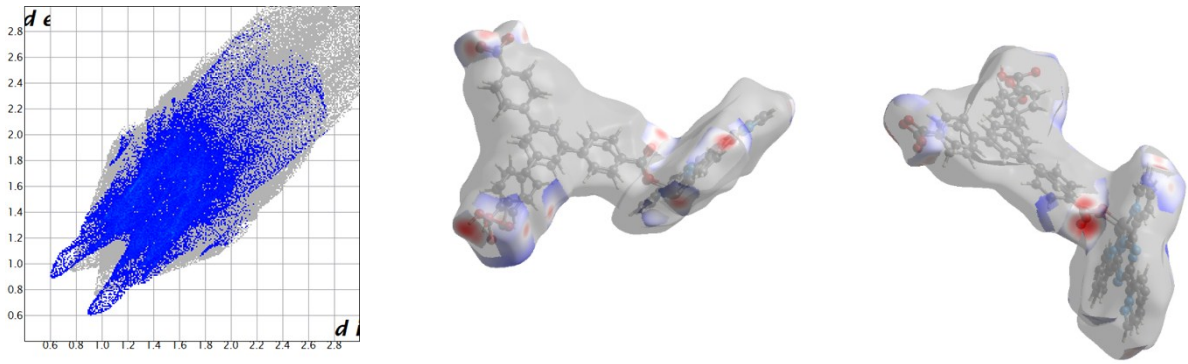

(d)

Figure S9: Fingerprint plots and corresponding regions plotted on the Hirshfeld surface for **2**: (a) Overall fingerprint plot, (b) C-C decomposed fingerprint and Dnorm plots, (c) C-H decomposed fingerprint and Dnorm plots (reciprocal contacts included), (d) O-H decomposed fingerprint and Dnorm plots (reciprocal contacts included).

In Fig. S9, the decomposed C-C plot shows that π-π interactions cover 5.0% of the total Hirshfeld surface. As in 1, the coloured region of the decomposed Dnorm surface correspond with A and B type stacking. The decomposed fingerprint for C-H and H-C short contacts accounts for 22.8% of the overall Hirshfeld surface. Hydrogen bonds are evaluated using the decomposed O-H and H-O fingerprint plot, and are localised on the surface at short contact regions around the pendant protonated carboxylate group and the oxygen atoms of the bound carboxylate. These cover 17.7% of the Hirshfeld surface.

(a)

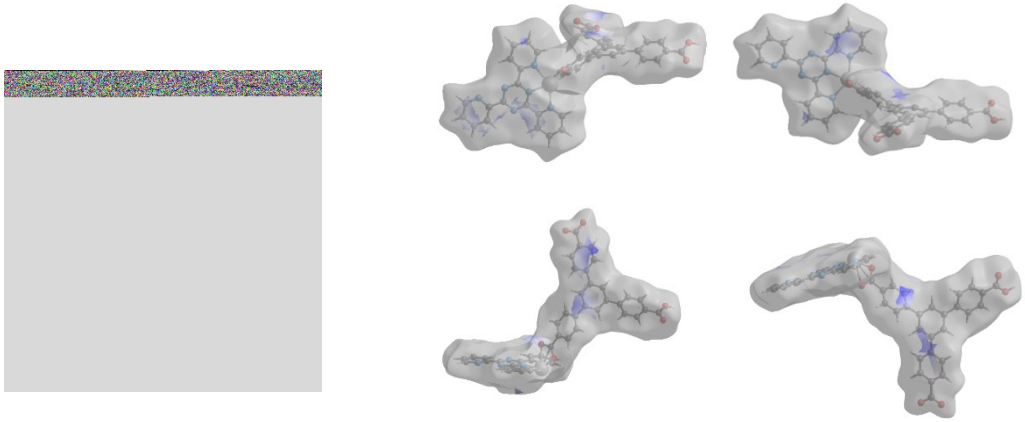

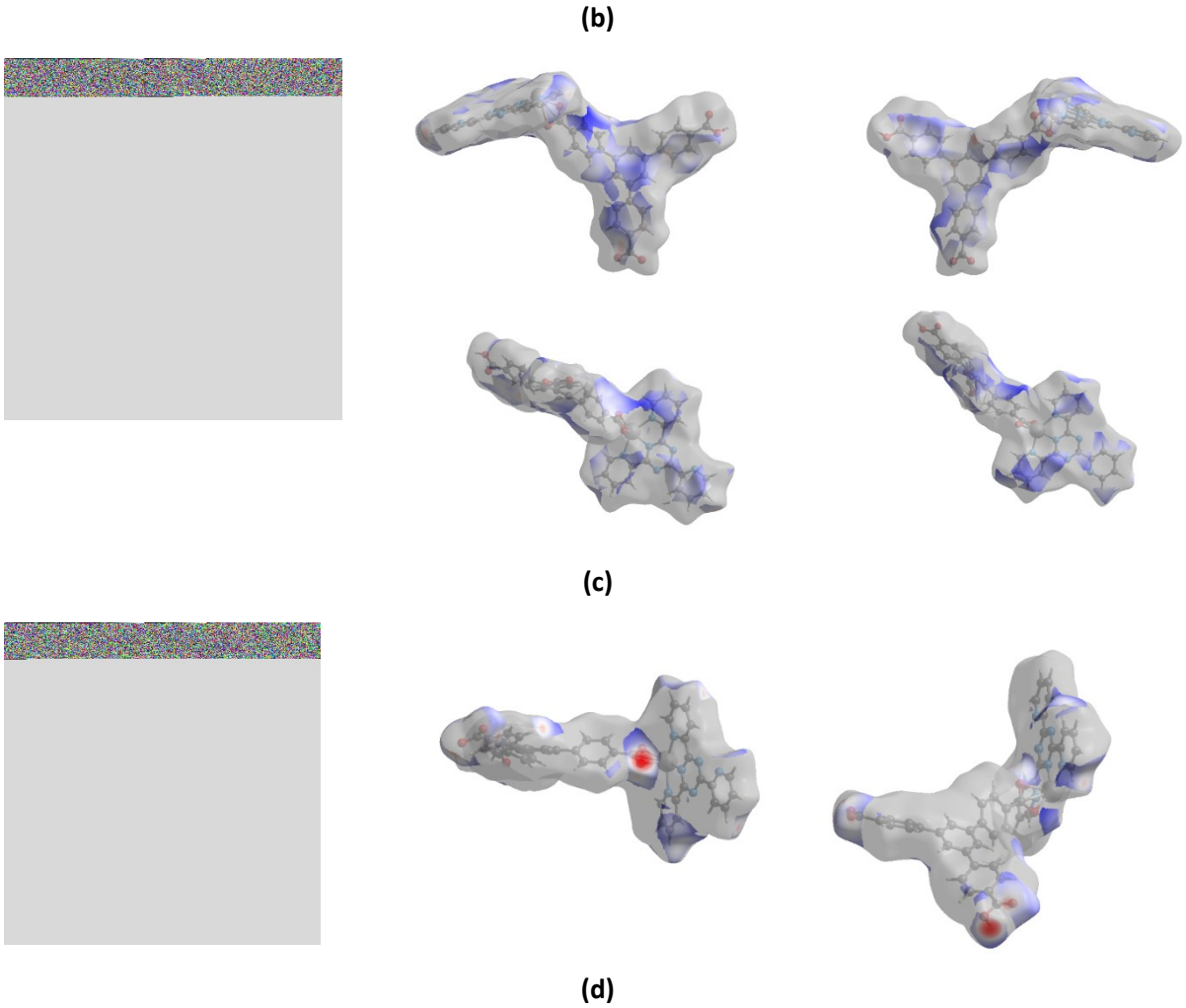

Figure S10: Fingerprint plots and corresponding regions plotted on the Hirshfeld surface for **3**: (a) Overall fingerprint plot, (b) C-C decomposed fingerprint and Dnorm plots, (c) C-H decomposed fingerprint and Dnorm plots (reciprocal contacts included), (d) O-H decomposed fingerprint and Dnorm plots (reciprocal contacts included).

In Fig. S10, the decomposed C-C plot shows that π-π interactions cover 5.3% of the total Hirshfeld surface. Here, the decomposed C-C surface shows evidence of A, B, and C type stacking modes. The decomposed fingerprint for C-H and H-C short contacts accounts for 28.1% of the overall Hirshfeld surface. Hydrogen bonds are evaluated using the decomposed O-H and H-O fingerprint plot, and are localised on the surface at short contact regions around the pendant protonated carboxylate group and the oxygen atoms of the bound carboxylate despite the bidentate mode now adopted. These cover 18.4% of the Hirshfeld surface.

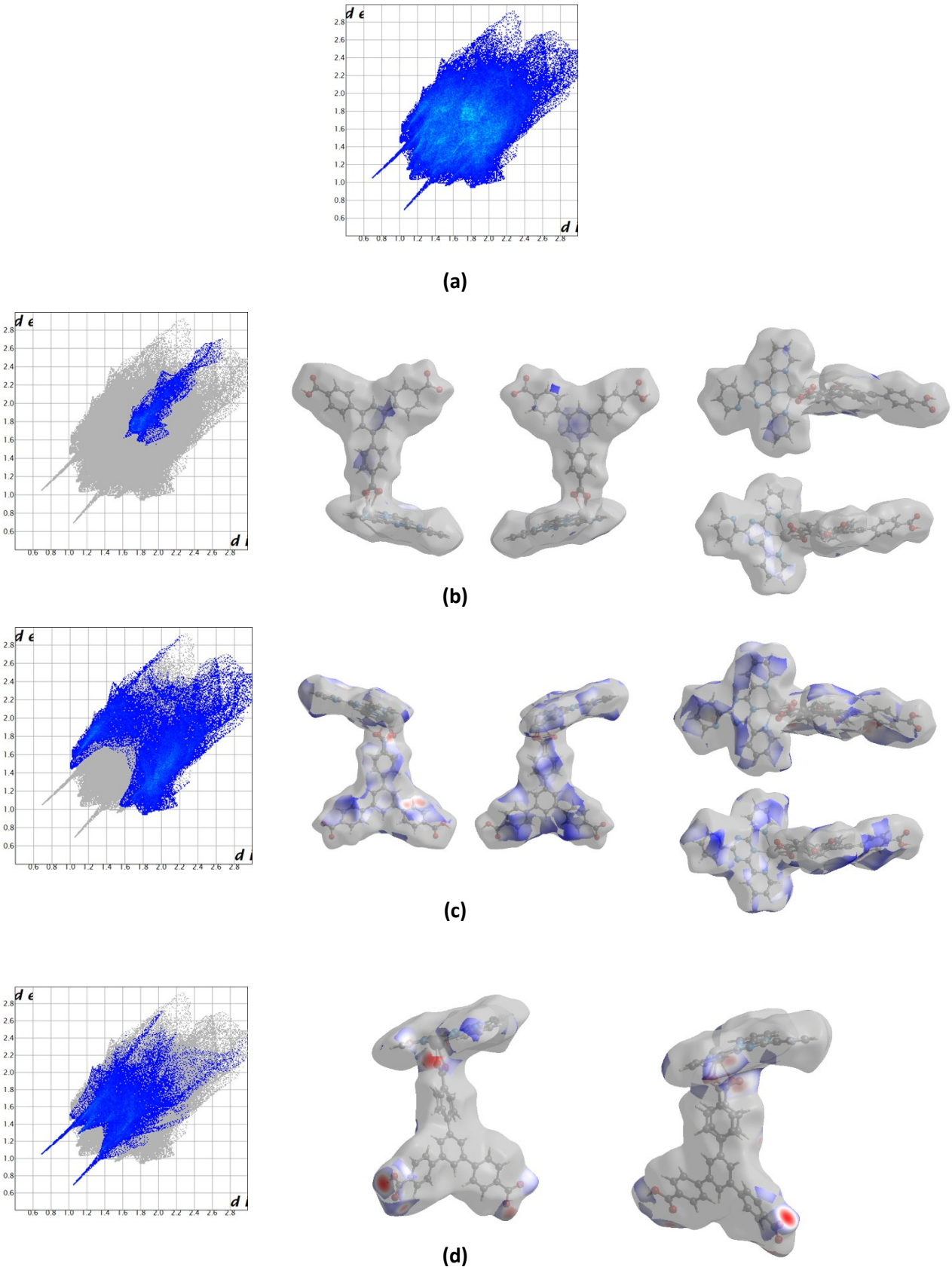

Figure S11: Fingerprint plots and corresponding regions plotted on the Hirshfeld surface for **4**: (a) Overall fingerprint plot, (b) C-C decomposed fingerprint and Dnorm plots, (c) C-H decomposed fingerprint and Dnorm plots (reciprocal contacts included), (d) O-H decomposed fingerprint and Dnorm plots (reciprocal contacts included).

In Fig. S11, the decomposed C-C plot shows that π-π interactions cover 5.3% of the total Hirshfeld surface, and the decomposed C-C surface shows evidence of A, B, and C type stacking modes. The decomposed fingerprint for C-H and H-C short contacts accounts for 32.2% of the overall Hirshfeld surface. Hydrogen bonds are evaluated using the decomposed O-H and H-O fingerprint plot, and are localised on the surface at short contact regions around the pendant protonated carboxylate group and the oxygen atoms of the bound carboxylate despite the bidentate mode now adopted. These cover 18.7% of the Hirshfeld surface.

Curvedness Plot

Curvedness as a function of the root mean curvature can be mapped on to the Hirshfeld surface with flat portions having low curvedness and areas that arc sharply having a high curvedness.[S9] Large flat regions on the curvedness plot corresponding to aromatic rings are observed (Fig. S19), which further indicate the prevalence of π-π interactions.[S10]

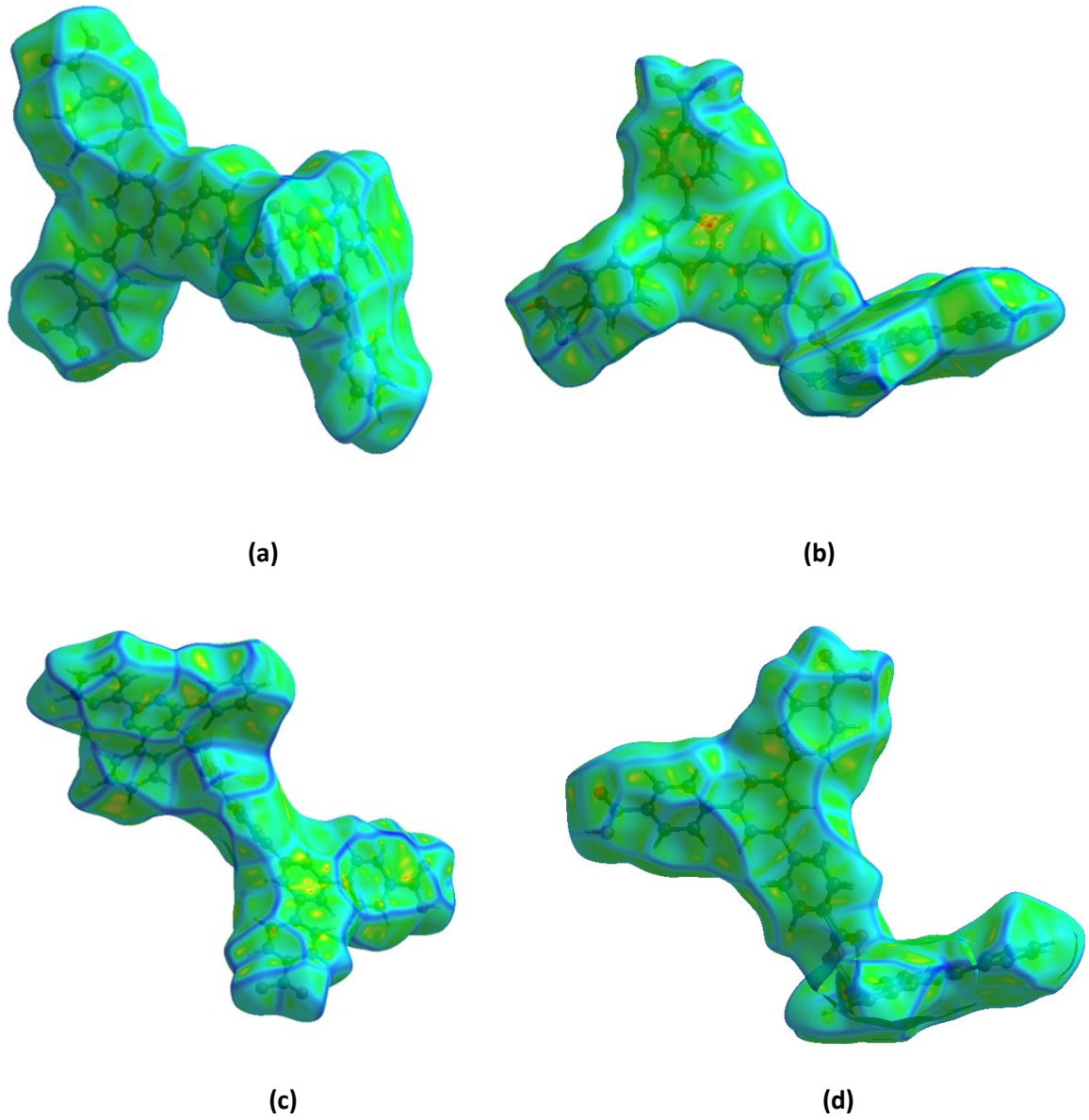

Figure S12: Curvedness plots of compounds **1**-**4**, respectively.

S8. References

[S1] Bruker AXS Inc., *SAINT+*, *Version 8.35*, 2012, Madison, Wisconsin, USA.
[S2] G.M. Sheldrick, *Acta. Cryst.* 2015, **A71**, 3-8.
[S3] O. V. Dolomanov, L. J. Bourhis, R. J. Gildea, J. A. K. Howard and H. Puschmann, *J. Appl. Crystallogr.*, 2009, **42**, 339-341.
[S4] G.M. Sheldrick, *Acta. Cryst.* 2015, **C71**, 3-8.
[S5] A. L. Spek, *Acta. Cryst.* 1990, **A46** . C34.
[S6] R. D. Shannon, *Acta Cryst.* 1976, **A32**, 751-767.
[S7] S.K. Wolff, D. Grimwood, J. McKinnon, D. Jayatilaka, M. Spackman, *Crystal Explorer*, **2005**, *Version 1.5.1.* University of Western Australia.
[S8] J.J. McKinnon, D. Jayatilaka, M.A. Spackman, *Chem Commun.* 2007, 3814-3816.
[S9] M.A. Spackman, J.J. McKinnon, *CrystEngComm* 2002, **4** ,378-392.
[S10] F. P. A. Fabbiani, D. R. Allan, S. Parsons, C. R. Pulham, *Acta Cryst.* 2006*,* **B62**, 826-842.